### Research Article

Tao Dong, Fengjia Gao, Quanmin Guo\*, Ding Chen, Linqiu Tan, and Lei Gong

# Optimization method for detection a flying bullet

https://doi.org/10.1515/phys-2022-0063 received April 21, 2022; accepted June 22, 2022

**Abstract:** With the rapid development of modern high technology and continuous improvement of production technology, stringent requirements have been imposed on modern barrel weapons in terms of precision, range, power, and mobility. This needs a substantial improvement and optimization of the detection equipment used to test the performance of barrel weapons. In the present work, an optimization method based on a light screen with a reflection for effectively and economically detecting bullets from barreled weapons within a large detection area is proposed. First, the detection principle of this system is described in detail. Next, the mathematical model of system detection performance is established. Then, the system is simulated, and the simulation results show the ability to realize the effective detection of a small projectile with a diameter of 5.8 mm through an area of  $10 \text{ m} \times 10 \text{ m}$ . The detection performance at different coordinates of the detection area is symmetrically distributed about the diagonal. Besides, the detection performance is improved with an increase in the bullet diameter and the laser power, respectively. Finally, an equal-scale reduction system with a detection area of 4 m × 4 m is constructed to perform a live ammunition shooting experiment. The distribution and variation of detection performance obtained experimentally are consistent with the simulation. Consequently, the proposed optimization method can meet the requirements concerning high detection performance, large detection area, and low cost.

**Keywords:** photoelectric test system, bullet detection, large detection area, reflective film, detection sensitivity

### 1 Introduction

Bullet velocity, firing accuracy, and firing rate are some important parameters in the performance evaluation of barrel weapons (i.e., pistols, rifles, machine guns, cannons, etc.). Generally, the above parameters can be accurately measured using various instruments such as sky screens [1-3], light screens [4-7], photoelectric arrays [8,9], and acoustic devices [10]. Moreover, high-tech barrel weapons with high velocity, high firing accuracy, and large lethal area are increasingly appearing in the military application field. Accordingly, the requirements for their measurement accuracy have also become more and more stringent. Unfortunately, existing detection methods still possess some limitations in detection capability, especially when working with large detection areas. For instance, the sky-screen systems have specific demands for the range of sky brightness, being unable to operate at night and in bad weather. In turn, the lightscreen detection system of a large detection area, in which the effective detection area is larger than  $3 \text{ m} \times 3 \text{ m}$ , is immature. Therefore, it is not suitable for detecting weapons with large bullet diameters. Besides, the receiver of a photoelectric array detection system is composed of multiple photodiodes spliced together. If the receiver is spliced into a large detection area, its structure will be very complex and difficult to install. Therefore, it is necessary to find an effective method to improve the detection performance of the bullet measurement systems; specifically speaking, a bullet of a certain caliber can be detected as far as possible within a larger detection area.

9

To solve this problem, several techniques have been proposed. In particular, the flight bullet detection methods based on the reflection principle have been introduced [11,12]. Generally, they all use reflective films, lasers, focus lenses, and photoelectric receivers to form a detection area with a fan shape. However, their effective detection area is smaller than  $1\,\mathrm{m}\times 1\,\mathrm{m}$ . In addition, some researchers have also put forward detection systems based on the photodiode arrays [13]. Such a system is composed of four lasers and a rectangular receiver. Especially, the receiver is spliced by many photodiodes. Because of the limitations of splicing technology, the maximum effective detection

<sup>\*</sup> Corresponding author: Quanmin Guo, School of Electronics Information Engineering, Xi'an Technological University, Xi'an 710021, China, e-mail: guoqm@163.com

Tao Dong, Fengjia Gao, Linqiu Tan, Lei Gong: Shaanxi Province Key Laboratory of Photoelectric Measurement and Instrument Technology, Xi'an Technological University, Xue-fu Middle Road, No. 2, 710021, Xi'an, China

Ding Chen: School of Armament Science and Technology, Xi'an Technological University, Xi'an 710021, China

area of the system is not beyond 1 m  $\times$  1 m. Moreover, other researchers have attempted to combine a sky-screen receiver and a light-emitting diode array light source to form a complex detection system [14]. This enabled them to extend the effective detection area to 10 m  $\times$  10 m. However, the light source is difficult to splice, and its uniformity is hard to adjust; besides, it is expensive.

In view of the above, the present research aims at improving the detection performance (mainly expanding the detection area) and simplifying the structure of the detection system. In particular, an optimization method using the light-screen reflection has been proposed. The detection performance of this setup is analyzed experimentally and via simulations, and the results are compared with the previously reported systems. The proposed technique enabled one to expand the effective detection area to  $10~\text{m} \times 10~\text{m}$ , thereby improving the detection performance in a cost-effective manner. Thus, it can meet the requirements for the detection performance of new barrel weapons.

## 2 Detection principle

### 2.1 System composition

Figure 1 displays the structure of the detection device under consideration. The proposed setup consists of a transmitter, a receiver, a reflective film, a frame, and a signal processing module. The transmitter comprises a spot continuous laser, a mirror, and a cylindrical lens, and its function is to form a thin fan-shaped light beam. The beam is subsequently emitted through the reflective film into the receiver, including a Fresnel lens and a PIN

silicon photodiode. The reflective film is a thin film that is attached to the frame. Its role is to reflect the light in the direction opposite to the incident beam direction. Consequently, the transmitter and receiver pair can structure a square detection area to effectively capture a flying bullet. For the selected spot continuous laser and PIN silicon photodiode, the laser wavelength should correspond to a peak response wavelength of the PIN silicon photodiode in the visible band. Therefore, we finally use a diode laser with a wavelength of 650 nm; certainly, this wavelength must also be within the effective spectrum range of the PIN silicon photodiode.

When a flying bullet passes through the detection area, it blocks a part of the light beam. Obviously, the energy received by the photodiode decreases, and then the signal processing module outputs a response signal. The amplitude of the response signal is defined as [15]

$$V(t) = \Phi(t)\varepsilon GR,\tag{1}$$

where  $\Phi(t)$  is the radiant flux blocked by the bullet,  $\varepsilon$  is the responsivity of the photodiode, G and R are the circuit gain and the conversion resistor of the signal processing module, respectively. Generally, the parameters  $\varepsilon$ , G, and R are constant after the circuit is determined. Consequently, the amplitude of the response signal V(t) is directly proportional to the blocked radiant flux  $\Phi(t)$ ; in other words, we study the detection performance of the system by analyzing the blocked radiant flux  $\Phi(t)$ .

### 2.2 Detection performance model

In this study, the thickness of the detection area is the same as the diameter of the laser spot, *i.e.*, 5 mm, which is shorter than the length of the common standard bullet. Therefore, we only discuss the detection performance

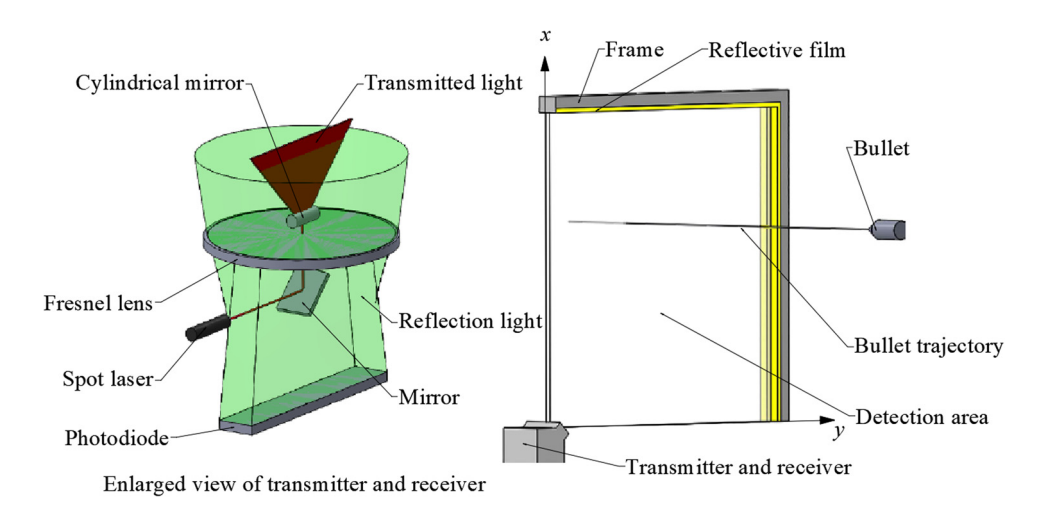


Figure 1: Schematic diagram of the proposed detection device.

under the condition that the length of the bullet is longer than the thickness of the detection area.

Figure 2 depicts the detection principle of the proposed system. We uniformly divide the reflective film into n segments. From left to right and from top to bottom, its center coordinates are denoted as  $(x_i, y_i)$  (i = 1, 2, ..., n). The length P of each segment and its area S' are, respectively, calculated as

$$P = 2l_1/n, \tag{2}$$

and

$$S' = 2l_1 d/n, (3)$$

where  $2l_1$  is the length of the reflective film and d is the diameter of the laser spot.

Furthermore, we analyze the light reflection at the ith segment of the reflective film. The dashed-dotted black line, the blue line, and the yellow lines represent the diagonal of the detection area, the direction of the light emitted by the transmitter, and the direction of the light reflected by the reflective film, respectively. In addition, angles  $\alpha_0$ ,  $\beta_i$ , and  $\gamma$  stand for the diffused angle of the cylindrical lens, the incidence angle, and the divergence angle of the reflective film of the ith segment, respectively (here and hereinafter, all angles are measured in radians).

The structure of the system is symmetric about the dashed-dotted line. For the upper left of the detection area, we analyze the geometric relationships and obtain

$$\begin{cases} x_i = 2l_1(i - 0.5)/n, \\ y_i = l_1, \end{cases}$$
 (4)

and

$$\beta_i = \tan^{-1}(x_i/y_i). \tag{5}$$

The laser source at O is originally a point source, but it can be expanded to an area source through a cylindrical lens. The size of the area source  $h_i$  is related to the distance from O to the center of the reflective film as follows [16]:

$$h_i = \sqrt{x_i^2 + y_i^2}, \qquad (6)$$

whereas the area

$$S_i = \alpha_0 dh_i = \alpha_0 d\sqrt{x_i^2 + y_i^2}. \tag{7}$$

According to the optical radiation property [17], the incident irradiance  $E_i$  and the incident radiant flux  $\Phi_i$  at the *i*th segment of the reflective film are respectively defined as

$$E_{i} = \frac{P_{0}\eta_{1}}{S_{i}} = \frac{P_{0}\eta_{1}}{\alpha_{0}d\sqrt{x_{i}^{2} + y_{i}^{2}}},$$
 (8)

and

$$\Phi_i = \frac{S' P_0 \eta_1}{S_i} = \frac{2l_1 P_0 \eta_1}{n \alpha_0 \sqrt{x_i^2 + y_i^2}},$$
 (9)

where  $P_0$  is the laser power and  $\eta_1$  is the photoelectric conversion efficiency of the laser.

In this study, a C00398 3M-2 type reflective film is used. When the light is incident on the reflective film, the reflection process of the light radiation energy will make a part of the loss. In addition, due to the manufacturing technique, the reflected light will inevitably have a small divergence angle  $\gamma$ . The ratio of the radiation energies of the reflected and incident light is called the reflectivity H of the reflective film. According to the experimental research, the divergence angle  $\gamma$  of the reflected light is 0.018 rad, and the reflectivity H of the reflective film is related to the incident angle  $\beta$ . Therefore, the reflectivity  $H_i$  can be found as follows:

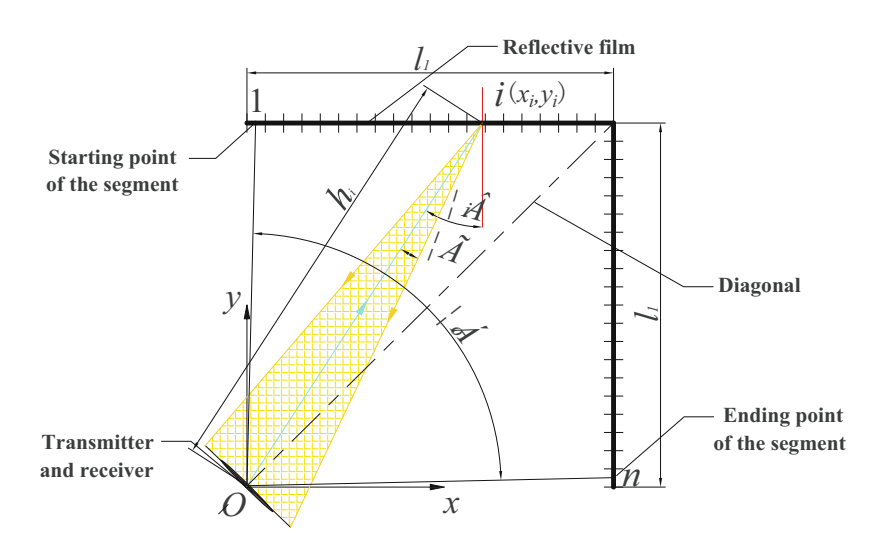


Figure 2: Schematic diagram of the detection principle of the proposed system.

$$H_i = 5.8 \times 10^{-8} \beta_i^5 - 5.957 \times 10^{-6} \beta_i^4$$

$$+ 1.8678 \times 10^{-4} \beta_i^3 - 0.0013 \beta_i^2$$

$$- 0.0272 \beta_i + 0.6715.$$
(10)

The reflected irradiance  $E'_i$  and the reflected radiant flux  $\Phi'_i$  at the ith segment of the reflective film can be respectively expressed as

$$E_i' = \frac{P_0 \eta_1}{S_i} = \frac{P_0 \eta_1 H_i}{\alpha_0 d \sqrt{x_i^2 + y_i^2}},$$
 (11)

and

$$\Phi_i' = \frac{S' P_0 \eta_1}{S_i} = \frac{2l_1 P_0 \eta_1 H_i}{n \alpha_0 \sqrt{x_i^2 + y_i^2}},$$
 (12)

As shown in Figure 3, the spot of the light, reflected by the ith segment of the reflective film to the surface of the Fresnel lens, can be regarded as a rectangle of the shadowed part. Besides, its length and width are denoted by  $d'_i$  and  $P'_i$ , respectively.

We assume that the aperture of the Fresnel lens is D, and then the received coefficient  $\eta_2$  of the Fresnel lens can be expressed as

$$P'_{i} = \left(\frac{2\sin\left(\frac{\pi}{2} - \gamma\right)}{\sin\left(\frac{\pi}{4} + \gamma\right)}\right) \times \left[x_{i} - \frac{x_{i}y_{i} - y_{i}^{2} \tan \gamma}{y_{i} + x_{i} \tan \gamma} + \frac{l_{1}}{n}\right],$$
(13)

$$d_i' = \left(\frac{2\sin\left(\frac{\pi}{2} - y\right)}{\sin\left(\frac{\pi}{4} + y\right)}\right) \times \left[x_i - \frac{x_i y_i - y_i^2 \tan y}{y_i + x_i \tan y} + \frac{d}{2}\right],$$
(14)

and

$$\eta_{2} = \begin{cases}
1, & P'_{i} < D, d'_{i} < D, \\
\frac{\pi D^{2}}{4} \left( 2\pi - 4 \arccos\left(\frac{d'_{i}}{D}\right) \right) + d'_{i} \sqrt{\left(\frac{D}{2}\right)^{2} - (d'_{i})^{2}} \\
P'_{i} > D, d'_{i} < D, \\
\frac{\pi D^{2}}{4} \left( 2\pi - 4 \arccos\left(\frac{P'_{i}}{D}\right) \right) + P'_{i} \sqrt{\left(\frac{D}{2}\right)^{2} - \left(\frac{P'_{i}}{2}\right)^{2}} \\
P'_{i} < D, d'_{i} > D \frac{\pi D^{2}}{P'_{i} d'_{i}}, \quad P'_{i} > D, d'_{i} > D.
\end{cases} (15)$$

When a bullet passes through the detection area, it blocks a part of the light beam emitted by the transmitter (see the yellow area in Figure 4). Therefore, the  $i_1$ - $i_2$  segments of the reflective film cannot receive the light emitted by the transmitter.

Assuming that the bullet coordinates in the detection area are  $(x_e, y_e)$  and the bullet diameter is  $d_e$ , the geometric relationship between the bullet and the reflective film can be established as

$$\begin{cases} x_{i1} = \frac{2l_{1}x_{e} - l_{1}d_{e}}{2y_{e}}, & y_{i1} = l_{1} \\ x_{i2} = \frac{2l_{1}x_{e} + l_{1}d_{e}}{2y_{e}}, & y_{i2} = l_{1} \end{cases}$$

$$\Rightarrow \begin{cases} i_{1} = \frac{n(2x_{e} - d_{e}) + 2y_{e}l_{1}}{4y_{e}l_{1}}, \\ i_{2} = \frac{n(2x_{e} + d_{e}) + 2y_{e}l_{1}}{4y_{e}l_{1}}, \end{cases}$$

$$(16)$$

where  $(x_{i_1}, y_{i_1})$  and  $(x_{i_2}, y_{i_2})$  are the center coordinates of the  $i_1$ th and  $i_2$ th segments, respectively.

Therefore, the blocked radiant flux  $\Phi'$ , which is blocked by the bullet for the  $i_1$ – $i_2$  segments, can be expressed as follows:

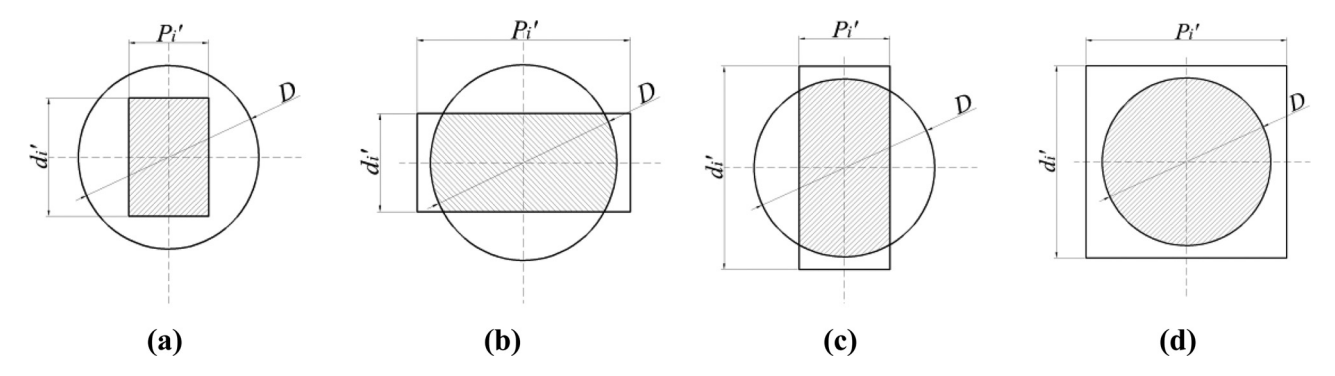


Figure 3: Calculation diagram of the received coefficient  $\eta_1$  of the Fresnel lens: (a)  $d_i' < D \& P_i' < D$ , (b)  $d_i' < D \& P_i' > D$ , (c)  $d_i' > D \& P_i' < D$ , (d)  $d_i' > D \& P_i' > D$ .

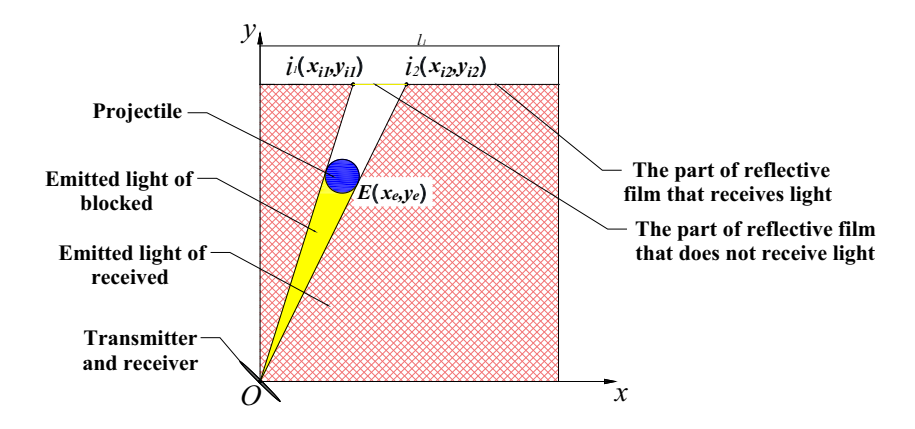


Figure 4: Diagram of the emitted light of blocked.

$$\Phi' = \sum_{i=i_1}^{i_2} \frac{2l_1 P_0 \eta_1 H_i \eta_2}{n \alpha_0 \sqrt{x_i^2 + y_i^2}}.$$
 (17)

The system detection performance  $\delta$  is linearly dependent on the blocked radiant flux  $\Phi'$  and can be written as follows:

$$\delta = \xi \cdot \Phi' = \sum_{i=i_1}^{i_2} \frac{2G l_1 P_0 \eta_1 H_i \eta_2}{n\alpha_0 \sqrt{x_i^2 + y_i^2}},$$
 (18)

where  $\xi$  is the gain factor of a circuit subsystem.

# 3 Detection performance simulation

According to the above models, the detection performance of the system is mainly affected by some key parameters such as the laser power, the length of the reflective film, and aperture of the Fresnel lens, and the hitting coordinates of the bullet and its diameter. In order to analyze the influence of various factors on the detection performance and to provide a theoretical basis for further optimization of the system, we perform the detection performance simulations by changing the bullet diameter, the bullet-hitting coordinates and the laser power, while keeping the other parameters constant.

Prior to the analysis, we have set some key system parameters (see Table 1). Among them, the diameter of the Fresnel lens is selected as 100 mm due to the limitation of manufacturing means and price. The wavelength of the laser should correspond to the photoelectric response peak of the reflection film, and it should be within the visible band to ensure convenient observation during the experiment. Since the photoelectric response peak band of the

reflection film used in this study is 960 nm, the laser wavelength is finally set as 650 nm. If the converted current of the photodiode is greater than 20 µA, the signal processing module will output a response signal. The responsibility of the photodiode is 0.5 A/W for the wavelength of 650 nm. Therefore, the bullet can be detected by the proposed system if the blocked radiant flux  $\Phi'$  is greater than 0.04 mW.

## 3.1 Detection performance vs bullet-hitting coordinates

To reveal the influence of different bullet-hitting coordinates on the detection performance, the blocked radiant flux  $\Phi'$  is afterward analyzed at different bullet-hitting coordinates by fixing the laser power  $P_0$  at 100 mW and the bullet diameter  $d_e$  at 5.8 mm.

The results of the simulation are shown in Figure 5. According to the graph, the blocked radiant flux  $\Phi'$  is symmetrically distributed about the diagonal in the detection area. When the  $x_e$ -coordinate is constant in the range

Table 1: Some key system parameters

Value
5.8
650
90
100
20,000
20,000
0.5

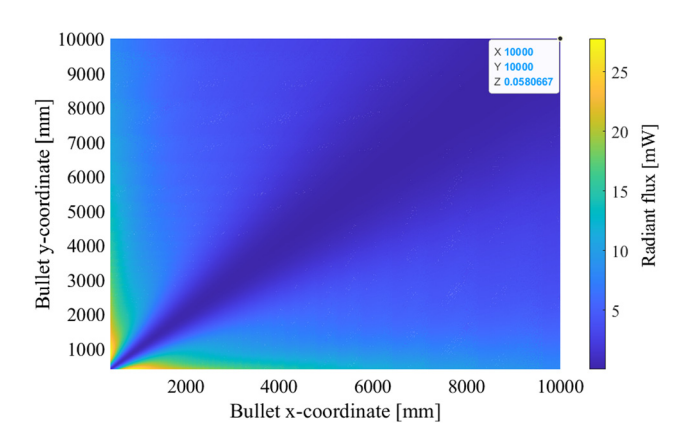


Figure 5: Blocked radiant flux  $\Phi'$  at different bullet-hitting coordinates.

from  $y_e = 0$  to  $y_e = x_e$ , the blocked radiant flux  $\Phi'$  decreases with increasing  $y_e$ -coordinate. Meanwhile, it increases as the  $y_e$ -coordinate further increases from  $y_e = x_e$  to  $y_e = 10,000$ . At the same time, when the  $y_e$ -coordinate is kept constant from  $x_e = 0$  to  $x_e = y_e$ , there is a decrease in the blocked luminous flux  $\Phi'$ . In turn, it increases with an increase in the  $x_e$ -coordinate from  $x_e = y_e$  to  $x_e = 10,000$ . Besides, the blocked radiant flux  $\Phi'$  is relatively low on the diagonal, achieving its minimum value of 0.058 mW at bullet-hitting coordinates of (10,000, 10,000). Since this value is slightly greater than 0.04 mW, the system can detect the bullet with a diameter of 5.8 mm in its detection area.

To sum up, the detection performance of a system under consideration is symmetrically distributed about the diagonal in the detection area. Specifically, the closer the distance to the diagonal, the worst the detection performance. For a bullet of a certain caliber, it allows one to avoid the detection blind area near the diagonal by selecting some reasonable parameters. In this case, the system can realize the effective detection of the bullet with a diameter greater than or equal to 5.8 mm within a detection area of  $10 \, \text{m} \times 10 \, \text{m}$  at the given system parameters.

# 3.2 Detection performance vs bullet diameter

The next stage of the study was to simulate the detection limit of the system depending on the bullet diameter. According to the above results at different bullet-hitting coordinates, the system has the lowest detection performance at the point (10,000, 10,000). Accordingly, we choose this point as the bullet-hitting coordinates and

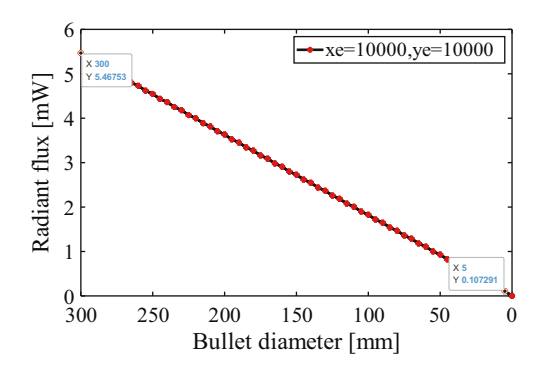


**Figure 6:** Blocked radiant flux  $\Phi'$  with different bullet diameters.

set the initial power of the laser at  $P_o = 100$  mW, whereas the diameter of the bullet is varied between 0 and 300 mm. Figure 6 displays the blocked radiation flux as a function of the bullet diameter at the hitting point (10,000, 10,000).

As seen in Figure 6, while the bullet diameter reduces from 300 to 5 mm, the blocked radiant flux  $\Phi'$  declines from 5.46 to 0.11 mW, *i.e.*, being still greater than 0.04 mW. Thus, the detection limit of the system for the bullet diameter is about 5 mm. Given some uncertainty factors, the minimum diameter of the measured bullet should be conservatively about 5.8 mm, which is the diameter of a standard-type bullet in the proposed system.

# 3.3 Detection performance vs the power of the laser

Below we determine the appropriate power of the continuous laser via simulations. First, we choose the farthest point relative to the point O with hitting coordinates (10,000, 10,000). Second, the diameter of the measured bullet  $d_e$  is fixed at 5.8 mm. Finally, the changes in system detection performance are observed at varying laser power between 5 and 200 mW to determine the most appropriate power according to the results. Figure 7 displays the blocked radiation flux as a function of the laser power at the bullet-hitting point (10,000, 10,000). While the continuous laser power goes down from 200 to 5 mW, the blocked radiant flux  $\Phi'$  declines from 0.11 to 0.0028 mW. As the laser power reaches a value of 75 mW, the blocked radiant flux  $\Phi'$  is 0.043 mW, i.e., being slightly greater than 0.04 mW, which is in line with the detection requirements. However, once the laser power goes below 75 mW, the blocked radiant flux  $\Phi'$  is less than 0.04 mW, which is beyond the detection standards.

Obviously, there is a change rule; that is, the greater the power of the laser, the larger the reflective radiant

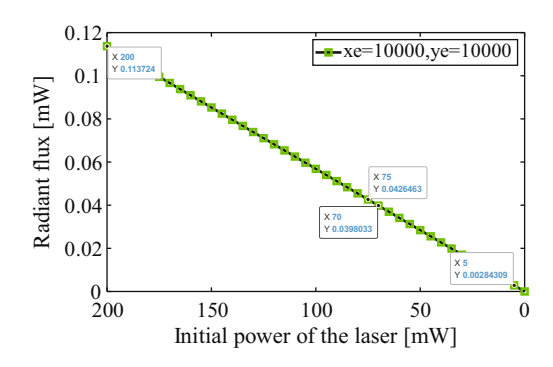


Figure 7: Blocked radiant flux  $\Phi'$  with a different power of the laser.

flux  $\Phi_i'$ , the greater the blocked radiant flux  $\Phi'$ , and thus the better the detection performance. Unfortunately, due to the increase in laser power, the laser beam volume also enlarges, which increases its cost. As a result, considering the power and volume of the laser beam, as well as the interference of the experimental environment and background light, a laser power of 80 mW should be the most optimal within a detection area of 10 m  $\times$  10 m.

## 4 Experiments and discussions

For the convenience of experiments, we set up an equal-scale reduction system with a detection area of 4 m  $\times$  4 m according to the established detection performance model. As seen from Figure 8, the transmitter and the receiver are placed in the lower-left corner of the system and the reflective film (shown in yellow in Figure 8) is attached to the frame, thereby forming a square detection area. Besides, a wooden board is placed at the rear 100 mm of the system, and a coordinate paper is also pasted on the board. Once a bullet is fired, the coordinates can be obtained by measuring the bullet-holes on the coordinate paper. The distance between the board and the system is shorter, and thus, the coordinates of the bullet-holes on the board can be approximately considered the bullet-hitting coordinates of the system.

### 4.1 Experiments

# 4.1.1 Detection performance vs bullet-hitting coordinates

We perform this experiment to verify the detection performance at different bullet-hitting coordinates. During

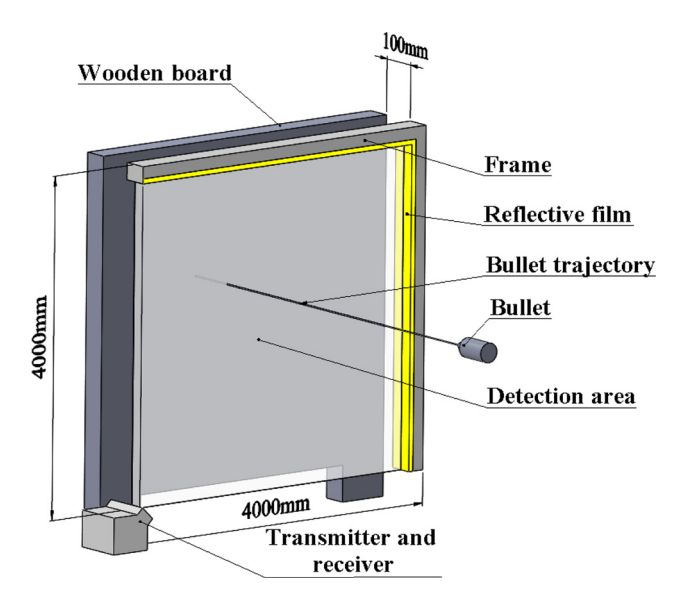


Figure 8: Experimental diagram of the equal-scale reduction system.

the experiment, the key system parameters are the same as in Table 1 and the power of the continuous laser is 50 mW. The test gun is horizontally fixed on a special gun rack, and the test bullet diameter is 5.8 mm, corresponding to the typical small-caliber standard bullet. The preset bullet-hitting coordinates are the black dots shown in Figure 9.

When a bullet is fired, we use an oscilloscope to display the waveform of the response signal of the system. The actual hitting coordinates  $(x'_e, y'_e)$  are obtained by measuring the position of the bullet holes on the coordinate paper. The actual hitting coordinates and the preset hitting coordinates exhibit a reasonable difference. In

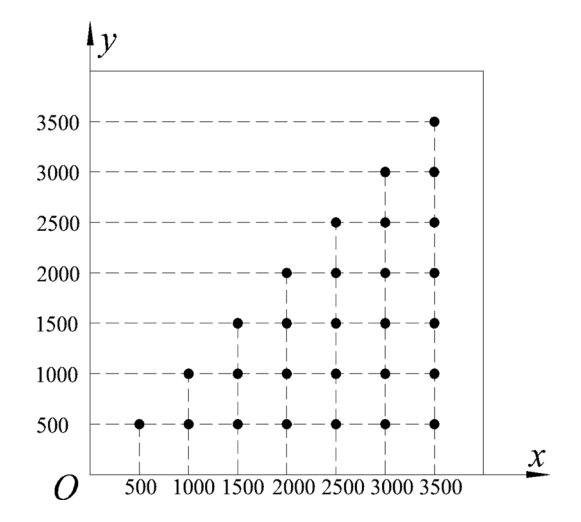


Figure 9: Schematic diagram of the bullet-hitting coordinates in the experiment.

Table 2: Experimental data at different bullet-hitting coordinates

The preset hitting coordinates	The actual hitting coordinates	Output amplitude V (V)	Average amplitude V <sub>A</sub> (V)	The preset hitting coordinates	The actual hitting coordinates	Output amplitude V (V)	Average amplitude V <sub>A</sub> (V)
$(x_e, y_e)$ (mm)	$(x_e', y_e')$ (mm)			$(x_e, y_e) \text{ (mm)}$	$(x_e', y_e')$ (mm)		
(500, 500)	(499, 500.5)	4.8	8.75	(2,000, 1,500)	(2,001, 1,499)	2.8	2.75
	(501, 498)	4.7			(2,002, 1,501)	2.7	
(1,000,500)	(999, 499)	7.6	7.7	(2,500, 1,500)	(2,502, 1,498)	2.8	2.9
	(1,002, 499)	7.8			(2,499, 1500.5)	3.0	
(1,500, 500)	(1,501, 501)	5.6	5.3	(3,000, 1,500)	(3,001, 1,499)	2.8	2.8
	(1,501, 498)	5.0			(2,999, 1,501)	2.8	
(2,000,	(1,998, 502)	4.8	4.8	(3,500, 1,500)	(3,502, 1,498)	2.4	2.45
500)	(2,001, 501)	4.8			(3,498, 1,498)	2.5	
(2,500,	(2499.5, 500)	4.4	4.3	(2,000, 2,000)	(1,999, 1,999)	1.6	1.55
500)	(2,502, 498)	4.2			(2,001, 2,000.5)	1.5	
(3,000,	(3,001, 502)	3.6	3.3	(2,500, 2,000)	(2,498, 1,999)	2.4	2.5
500)	(3,002, 498)	3.0			(2,501, 1,998)	2.6	
(3,500,	(3,499, 500.5)	3.2	3.0	(3,000, 2,000)	(2,999, 2,000)	2.2	2.1
500)	(3,501, 498)	2.8			(3,001, 2,001)	2.0	
(1,000,	(1,001, 999)	2.2	2.1	(3,500, 2,000)	(3,501, 1,999)	2.2	2.0
1,000)	(998, 1,000)	2.0			(3,502, 1,999)	1.8	
(1,500,	(1,500, 1,001)	4.8	5.0	(2,500, 2,500)	(2,502, 2500.5)	1.4	1.35
1,000)	(1,501, 1,000)	5.2			(2,498, 2,499)	1.3	
(2,000,	(2,001, 1000.5)	3.6	3.7	(3,000, 2,500)	(2,999, 2,499)	1.8	1.9
1,000)	(1,999, 999)	3.8			(2,998, 2,498)	2.0	
(2,500,	(2,499, 1,000)	3.4	3.4	(3,500, 2,500)	(3,501, 2,500)	1.8	1.7
1,000)	(2,500, 1,001)	3.4			(3,501, 2,502)	1.6	
(3,000,	(3,000, 999)	3.1	3.05	(3,000, 3,000)	(3,001, 3,000)	1.2	1.25
1,000)	(3,001, 1,002)	2.9			(2,999, 2,999)	1.3	
(3,500,	(3,498, 998)	2.6	2.5	(3,500, 3,000)	(3,500, 2,998)	1.6	1.5
1,000)	(3,502, 999)	2.4			(3,500, 3,001)	1.4	
(1,500,	(1500.5, 1,499)	1.7	1.65	(3,500, 3,500)	(3500.5, 3,499)	1.0	0.95
1,500)	(1,499, 1,501)	1.6			(3,501, 3,501)	0.9	

addition, when the key system parameters and the bullet diameter are constant for the lower right of the detection area, the experimental data are as shown in Table 2. A part of the waveform response signal generated by the oscilloscope during the experiment is shown in Figure 10.

When the  $y_e$ -coordinate is 500 mm, the output amplitude of the response signal decreases with the increase of  $x_{\rm e}$ -coordinate from  $x_{\rm e}$  = 1,000 to  $x_{\rm e}$  = 3,500. The same trend is observed at the  $x_e$ -coordinate of 3,500 mm with the increase of  $y_e$ -coordinate from  $y_e$  = 500 to  $y_e$  = 3,500.

Moreover, the output amplitude of the response signal rapidly decreases with a simultaneous increase of the bullet-hitting  $x_{e^-}$  and  $y_{e^-}$  coordinates on the diagonal of the detection area. Moreover, it achieves its minimum at the bullet-hitting coordinates (3,500, 3,500). The output amplitude of the response signal is about 0.95 V, and it can be distinguished from noise. Therefore, the system can detect the bullet with the diameter of 5.8 mm in a detection area of  $4 \text{ m} \times 4 \text{ m}$ .

In conclusion, when the bullet hits the points on the diagonal of the detection area, the larger the distance from these points to the laser, the smaller the output amplitude of the response signal. The least output amplitude of the response signal is attained at the point (3,500, 3,500). For the lower right of the detection area, the output amplitude of the response signal decreases with the increase of the bullet-hitting  $x_{e^-}$  and  $y_{e^-}$  coordinate, respectively. Therefore, the simulation results are consistent with the experimental data.

#### 4.1.2 Detection performance vs bullet diameter

The purpose of this experiment is to investigate the system detection performance for bullets with different diameters. The key system parameters are same as in Table 1 and the laser power is 50 mW. We have horizontally fixed the test gun on a special gun rack and shoot

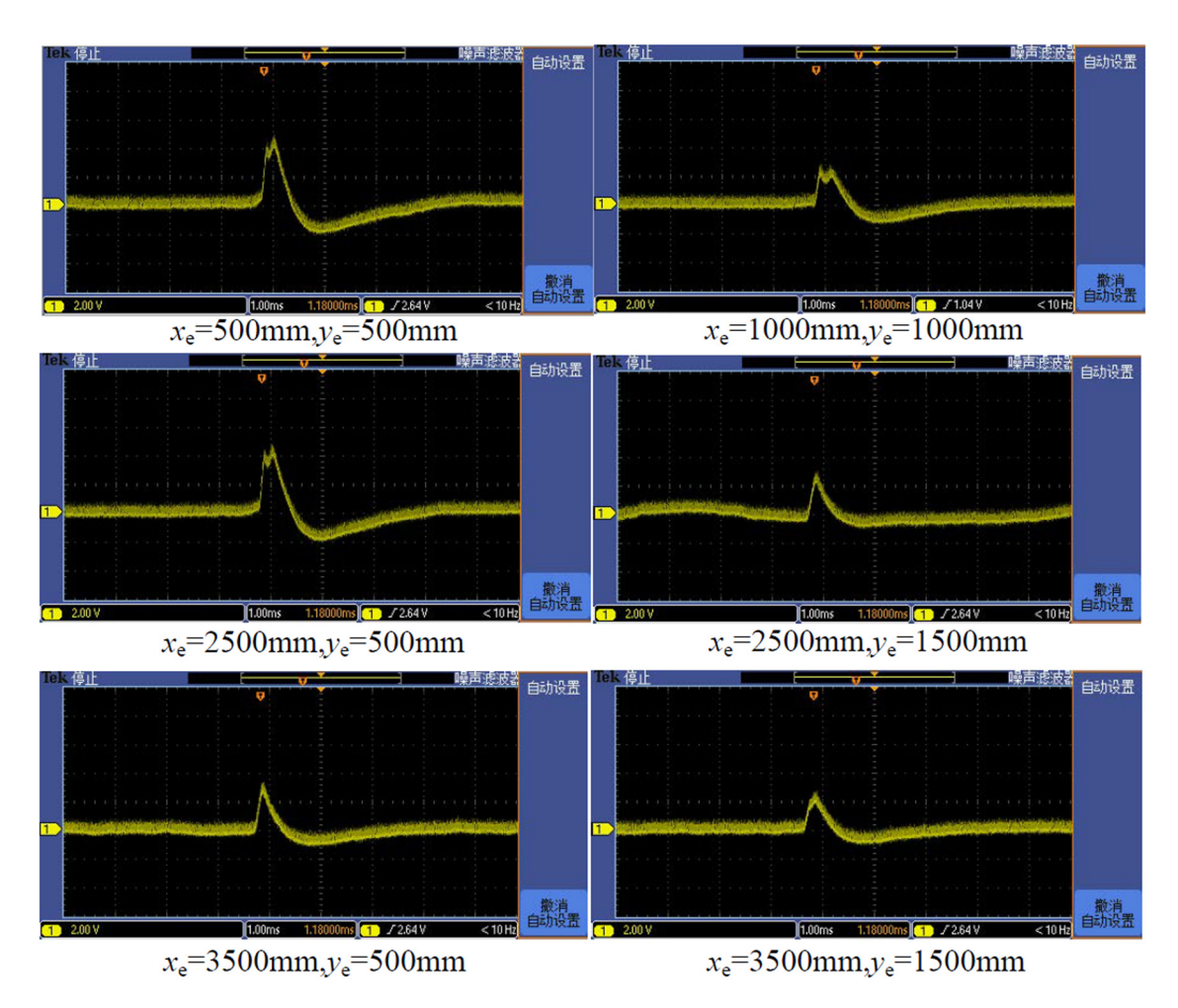


Figure 10: A part of the waveform response signal at different bullet-hitting coordinates.

the typical standard bullet with different bullet diameters at the preset coordinate (3,500, 3,500). Then, we use an oscilloscope to display the waveform of the response signal. Besides, the experimental data with reasonable errors are retained, as shown in Table 3.

According to the above analyses, when the key system parameters and the bullet-hitting coordinates are constant, the output amplitude of the response signal increases with an increase of the bullet diameter. Thus, the detection performance is improved with an increase in the bullet diameter. The results are consistent with those obtained in the previous section.

### 4.1.3 Detection performance vs laser power

This experiment is carried out to verify the system detection performance with a different laser power. The key

Table 3: Experimental data with different bullet diameters

diameter d <sub>e</sub> (mm)	Output amplitude <i>V</i> <sub>1</sub> (V)	Output amplitude V <sub>2</sub> (V)	Average amplitude V <sub>A</sub> (V)	
5.8	1.0	1.2	1.1	
7.62	1.4	1.6	1.5	
12.7	2.3	2.2	2.25	
14.5	2.7	2.9	2.8	

Table 4: Experimental data with different laser powers

Laser power P <sub>o</sub> (mW)	Output amplitude <i>V</i> <sub>1</sub> (V)	Output amplitude V <sub>2</sub> (V)	Average amplitude <i>V</i> <sub>A</sub> (V)
150	3.4	3.2	3.3
100	2.1	2.0	2.05
80	1.6	1.8	1.7
50	1.1	1.1	1.1

system parameters are the same as in Table 1 and the laser power are set at 50, 80, 100, and 150 mW. We have horizontally fixed the test gun on the special gun rack and shoot the typical standard bullet with a diameter of 5.56 mm at the coordinates (3,500, 3,500). Then, we use an oscilloscope to display the waveform of the response signal. Besides, the experimental data, which have a reasonable error between the actual and preset hitting coordinates, are preserved, as shown in Table 4.

According to the data, when the key system parameters, the bullet-hitting coordinates and the bullet diameter are kept constant, the output amplitude of the response signal decreases with a decrease of laser power. Obviously, the detection performance is improved with increasing laser power. In addition, when the power of the laser is 150 mW, the volume of the laser is large, and it also brings about inconvenient installation. In turn, a laser power of 50 mW enables one to achieve the output amplitude of the response signal of about 1.1 V, which is close to the limit of identification. In this respect, the laser power and detection requirements should be considered comprehensively. If the detection area is  $4,000 \, \text{mm} \times 400 \, \text{mm}$ , the most optimal laser power is 50 mW.

#### 4.2 Discussions

Through the simulations and experiments, the proposed system can effectively detect bullets whose diameters are greater than or equal to 5.8 mm in a detection area of  $10 \text{ m} \times 10 \text{ m}$  at the given system parameters. According to these results, a higher detection performance could be achieved, if compared to other reported appliances. For instance, the bullet detection limit was substantially increased over those attained in refs. [11,12], in which the bullet with a diameter of 5.8 mm could be detected within a detection area of  $0.5 \,\mathrm{m} \times 0.5 \,\mathrm{m}$ . Also, the photodiode array in ref. [13] was able to detect the bullet with a diameter of 7.62 mm in a detection area of  $1 \text{ m} \times 1 \text{ m}$ . Finally, the bullet with a diameter of 5.56 mm only was captured in a detection area of  $10 \text{ m} \times 10 \text{ m}$  using the sky screen or the light screen in ref. [14]. Moreover, unlike the previous methods, the proposed system is attractive for its simpler structure, more convenient installation and lower cost.

### 5 Conclusions

An optimization method was proposed to effectively improve the detection performance for a flying bullet using a light-

screen reflective system, which would accomplish the stringent requirements for advanced weapons. Based on the detection principle of the system, the model of detection performance was established, analyzed and verified. Based on the simulation and experimental data, the conclusions can be drawn as follows. First, the detection performance was symmetrically distributed about the diagonal in the detection area. Second, the detection performance depended on the bullet-hitting coordinates on the diagonal within the detection area: the larger the distance from the coordinates to the laser, the worst the detection performance. Furthermore, the detection performance was improved with an increase of the bullet diameter and the laser power, respectively. At last, the system was shown to be able to effectively detect bullets whose diameter is greater than or equal to 5.8 mm in the detection area of  $10 \text{ m} \times 10 \text{ m}$ . Therefore, this study provides a theoretical basis for developing of the detection performance models of photoelectric measurement setups using the light-screen reflective systems. Besides, the designed system also has a higher application value at a lower cost, and further improving the uniformity of its detection performance will be within the scope of our future research.

**Funding information:** This work was supported by the Young Scientists Fund of the National Natural Science Foundation of China granted No. 61905187, the Shaanxi Provincial Key Research and Development Program (no. 2019GY-094), and the Shaanxi Provincial Education Department (Scientific Research Program no. 20JS059).

Author contributions: All authors have accepted responsibility for the entire content of this manuscript and approved its submission.

Conflict of interest: The authors state no conflict of interest.

### References

- Li H. Research on space target detection ability calculation method and spectral filtering technology in sky-screen's photoelectric system. Microw Optical Technol Lett. 2016;58(5):1035-41.
- Musayev E. Laser-based large detection area speed measurement methods and systems. Opt Lasers Eng. 2007;45(11):1049-54.
- Akahoshi Y, Kaji M, Hata H. Meaurement of mass. spray angle and velocity distribution of fragment cloud. Intern J IMPACT Eng. 2003;29:845-53.

- Chu W, Zhang B, Liu B, Gui Z, Zhao D. An optoelectronic targeting system for measuring the distribution of projectile motion based on the subdivision of a light screen. Photonics. 2019;6(4):126.
- Musayev E. Optoelectronic methods and devices for measuring bullet velocity. J Meas Tech. 2006;49(3):270-5.
- Biswal TK, Sarkar S, Adhikary M. Feasibility study of virtual target scoring using high-speed imaging techniques. Propellants Explos Pyrotech. 2013;38(4):511-4.
- [7] Wang F, Ni J, Tian H, Yang T. Light transmission characteristic analyses of a laser screen in clear water based on the Monte Carlo method. Appl Opt. 2020;59(22):6625-31.
- Musa E, Demirer, M. Laser-based light barrier having a rectangular detection area. Opt Lasers Eng. 2010;48(4):435-40.
- Ni JP, Yang L. Method for measuring velocity of warhead fragments based on photoelectric detection. J China Ordnance. 2007;3(4):275-80.
- [10] Sedunov A, Sutin A, Salloum H. J J Acoust Soc Am. 2013;134(5).
- [11] Zhao D, Zhou H, Liu J, Zhang B, Luo Q. Enhanced antimicrobial properties, cytocompatibility, and corrosion resistance of

- plasma-modified biodegradable magnesium alloys. Optik. 2013;124(6):544-56.
- [12] Fang W, Changan D, Yunfei J, Li W. Light transmission characteristics analyses of laserscreen in clear water based on monte carlo method. Transducer Microsyst Technol. 2009;12:17.
- [13] Qiu W. Optical Engineering. MS. thesis. Taiyuan: North University of China; 2013.
- [14] Hui T, Yun Y, Ding C. Improvement of the detection sensitivity uniformity of an indoor light screen array measurement system with large field of view angle using multi-lens splicing. Optik. 2019;181:971-7.
- [15] Ni J. Technology and application of measurement of the light screen array. Chap. 2. Beijing: National Defense Industry Press; p. 25-71.
- [16] Shunxiang S, Xueen W, Lin M. Physical optics and applied optics. Chap. 10. Xi'an: Xidian University Press; p. 459-67.
- [17] Jun H, Yun L. Optical engineering. Chap. 6. Beijing: National Defense Industry Press; p. 65-70.